Case Studies in Thermal Engineering 35 (2022) 102082

Contents lists available at ScienceDirect

Case Studies in Thermal Engineering

journal homepage: www.elsevier.com/locate/csite

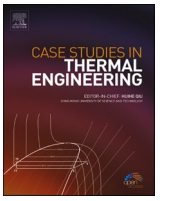

Experimental investigation on end winding thermal management with oil spray in electric vehicles

Xuehui Wang [a], Bo Li [a], Kuo Huang [a], Yuying Yan, PhD [a,*], Ian Stone [b], Sean Worrall [b]

[a] Fluids and Thermal Engineering Research Group, Faculty of Engineering, University of Nottingham, NG7 2RD, UK
[b] GKN Innovation Centre, Abingdon, Abingdon, Oxford, OX14 3PZ, UK

ARTICLE INFO

Keywords:
Spray cooling
End winding
Electric motor
Winding
Thermal management

ABSTRACT

To achieve a carbon-neutral sustainable future, the transportation sector is experiencing quick electrification, as more and more vehicles are driven by electric motors. Electric motors are designing more and more powerful and thus pose a great increasing challenge for thermal management. In this paper, an innovative experimental study on oil spray for end winding thermal management were presented. The experimental results indicated that the oil spray cooling significantly decrease the temperature of the winding. With higher oil temperature and flow rate, better cooling performance and better temperature uniformity were achieved both for teeth and slot winding. Meanwhile, a heat transfer performance prediction model based on a fully connected artificial neural network (ANN) was developed to correlate oil spray. The model used Reynolds number and Prandtl number as inputs, and the number of neurons in hidden layer was optimized to 8. The model accurately predicts the heat transfer performance of oil spray with a correlation coefficient of 0.93. The paper is expected to be a good reference for the oil spray engineering application in e-motor cooling.

Nomenclature

A	area (m^2)
a	thermal diffusivity (m^2/s)
b	bias
D	variance
E	identity matrix
e	error
f	function
H	Hessian matrix
h	heat transfer coefficient ($W/m^2 \bullet K^{-1}$)
J	Jacobian matrix
MSE	mean square error
Nu	Nusselt number
Pr	Prandtl number

* Corresponding author.
E-mail address: Yuying.Yan@nottingham.ac.uk (Y. Yan).

https://doi.org/10.1016/j.csite.2022.102082
Received 6 January 2022; Received in revised form 23 April 2022; Accepted 29 April 2022
Available online 4 May 2022

Δp	pressure drop (Pa)
Q	heating power (W)
Re	Reynolds number
r	correlation coefficient
T	temperature (°C)
V	velocity (m/s)
x	input
y	output

Greek symbols

λ	thermal conductivity(W/(m•K))
υ	kinematic viscosity (m^2/s)
w	weight
ρ	density (kg/m^3)

subscript

ew	end winding
exp	experiment
min	minimum
max	maximum
o	oil
pre	prediction

1. Introduction

With increasing concerns about climate change, more and more governments, international organizations, companies have released their commitments to achieve the carbon neutrality by around the middle of this century [1–3]. Against this background, the transportation sector is experiencing rapid electrification worldwide to cut off the consumption of fuels and oils [4,5]. More and more vehicles will be driven by electric motors. It is predicted that by 2030, 30% of the new sale cars will be electric cars [6]. To make electric cars more competitive, the motor is designing more and more powerful, with higher torque, higher speed and higher power density. As a result, it poses a great challenge to thermal management [7–9]. Generally, a motor is a very complex thermal network system. There are distributed heat sources in a quite compact space, and the heat losses include copper loss, iron loss, magnet loss, mechanical loss and stray loss due to different physical mechanisms. Furthermore, there are copper, carbon steel and resin used for motor components, whose optimal working temperature and safety temperature limits are also different [9,10]. Elaborate thermal management technics involving heat conduction, convection and even radiation heat transfer are needed to redistribute the heat and meet the cooling requirements. The failure of motor thermal management will cause lots of issues, including the ageing of the winding insulation, a shorter expectancy, a lower efficiency electric short circuit and even burnout of the motor [11,12]. For popular permanent-magnet motors in electric cars, the magnets with rare-earth metals in the rotor will also suffer from irreversible demagnetization caused by high temperature [13].

Currently, although air [14–16] and water jacket cooling [17–20] are also widely used for thermal management of motors, they can't satisfy severe requirements of higher heat flux of motors in the coming future, due to the poor thermal conductivities of the lamination and insulation materials. Most heat generates in the winding by the Joule effect. From this point of view, cooling methods that directly target the winding will surely dissipate the heat efficiently. Recent advanced cooling methods are based on this concept and novel research have been conducted. As the winding in the slot, Lindh et al. [21] combined cooling tubes with the slot winding and tested its performance with three real drive cycles. It was reported that the maximum temperature of the winding was only 77 °C, well below the safety temperature limit of the motor components. Liu et al. [22] compared the performance of water jacket cooling and direct winding cooling. It was concluded that with the winding cooling, the thermal resistance was reduced by 80% as well as the continuous torque output tripled. Reinap et al. [23] reported the current density of the slot winding doubled with oil direct cooling, comparing with air convection cooling. Xu et al. [24] also confirmed the important role of cooling tubes inside of the slot with the winding, along with the suggestion that evenly distribution of the tubes benefited the cooling performance. Direct cooling for the end winding is another prospective method for thermal management considering more space is available. Li et al. [25] investigated the end winding oil cooling under stagnant and flowing states by separating the rotor and stator through a well-sealed glass fiber sleeve. It was found that the temperature of the end winding was reduced by 43.6 °C compared with the cooling with water jacket only when two ends of end winding are immersed by still oil. Madonna et al. [26,27] introduced a noninvasive cooling pipe network for thermal management of end winding. The cooling pipe was directly placed onto the end winding surface to dissipate the heat. It was presented that with the end winding cooling, a 25% reduction of end winding temperature was achieved. The spray cooling, especially, is also under critical consideration apart from convection cooling. Liu et al. [28] conducted an experimental investigation on end winding cooling by oil spray. It was suggested that with oil spray, the current density and motor output almost doubled. The influence of the spray parameters and nozzle configuration was also discussed. Li et al. [29] compared the cooling of the water jacket and oil spray

cooling. It was found that with the hybrid cooling method, the temperature of the motor was well decreased by 40%–50%, as well as the response time reduced by 30%–60%. Guechi et al. [30] developed a CFD model to analyze the prospect of spray cooling for the end winding. The results also highlighted the advantages of spray cooling. Generally, the research with respect to two nominate winding configurations (random and hairpin windings), middle-to-high heat flux regime against the convection heat transfer cooling has been reported.

Despite the spray cooling has a very good prospect for thermal management of motors as indicated, the heat transfer characteristics and thermal modeling has not been fully investigated. How to maximize oil spray cooling and optimize heat transfer performance are still need more comprehensive studies. To further understand the heat transfer characteristics of oil spray cooling and the related optimization, in this work, an innovative experimental study for the oil spray cooling on end winding were presented. The influence of operational parameters of the oil spray was discussed, followed by a fully-connected ANN model to correlate the heat transfer of oil spray, targeting to the optimization of motor thermal management with end winding spray cooling.

2. Experiment

2.1. Experimental rig

To investigate the performance of oil spray cooling, a test rig was developed as shown in Fig. 1. The experimental rig consisted of a stator module, a heating module, a cooling module and a data acquisition module. Considering the symmetric characteristics of the stator, only 1/3 of the stator was made. The geometric dimensions of the stator section are presented in Table 1. A programmable DC power supply was used to heat the winding, whose electric resistance was 5.5 Ω. The heating power was recorded by a power supply. The cooling oil from the oil chiller with a temperature-control accuracy of 0.1 °C was pressurized by a gearbox pump. For each side of the end winding, there are two spray nozzles. The distance between the end winding and nozzle outlet was set at 70 mm.

The flow rate of the oil was measured by an electromagnetic flowmeter with an accuracy of 0.1 L/min. The pressure and temperature of the oil were further collected at inlets of the nozzles. Meanwhile, the temperatures of the yoke, teeth, slot winding, and end winding were also recorded by a series of T-type thermocouples. To identify the temperature gradients of the slot winding and teeth, there were five thermocouples evenly distributed in the axial direction. The accuracy of the thermal couples was calibrated to be ±0.2 K. The temperature and pressure data were recorded by the Agilent 34970A, whose accuracy was $6^{1/2}$.

The nozzles used were full-cone nozzles with S-shape internal vanes. The inner diameter of passage and spray angle at 3 bar were 0.94 mm and 51°, respectively. There were two nozzles at each end of end winding, as shown in Fig. 1.

The essential thermodynamic properties of the oil tested in the experiment are given in Table 2. The investigated ranges of heating power, oil temperature, oil flow rate and pressure were (60–780) W, (40–58) °C, (1.8–3) L/min and (1–3) bar, respectively.

2.2. Data reduce

To identify the performance of oil spray cooling for the end winding, temperatures of stator regime and parameters of oil were collected as mentioned before. Due to the configuration of cooling, the highest temperatures of teeth and slot winding are in the middle. Therefore, the temperature gradients of the winding and teeth are very important indexes, and are given by,

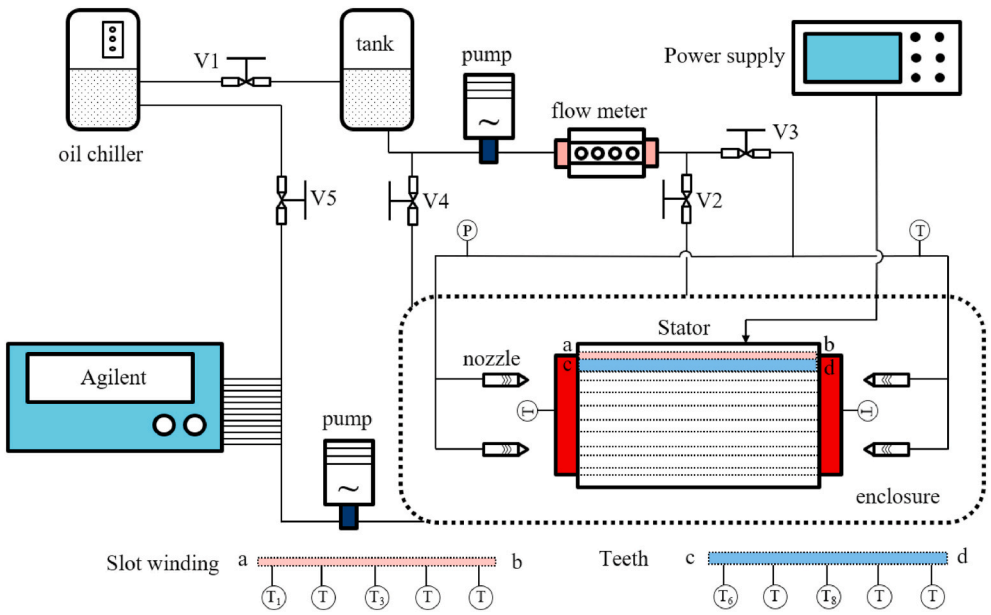

Fig. 1. The schematic diagram of the test rig.

Table 1
The dimensions of the tested stator section.

Parameters	Values
length of the motor	93 mm
number of teeth	6
width of teeth (average)	11.98 mm
diameter of the teeth	179.2 mm
diameter of stator	216.7 mm
diameter of teeth root	134.7 mm
winding diameter	0.9 mm
filling ratio of slot	~0.5

Table 2
The thermodynamic properties of the oil.

Ref. temperature	Thermal conductivity (W/(m• K))	Viscosity (m^2/s)	Density (kg/m^3)	Heat capacity (kJ/kg• K)
50 °C	0.135	1.55×10^{-5}	823.9	2.00

$$dT_{sw} = T_3 - T_1 \tag{1}$$

$$dT_t = T_8 - T_6 \tag{2}$$

The heat transfer performance of the oil is correlated by,

$$Nu = f(Re, Pr) \tag{3}$$

where *Nu*, Re and Pr are Nusselt number, Reynolds number and Prandtl number and calculated by the following equations,

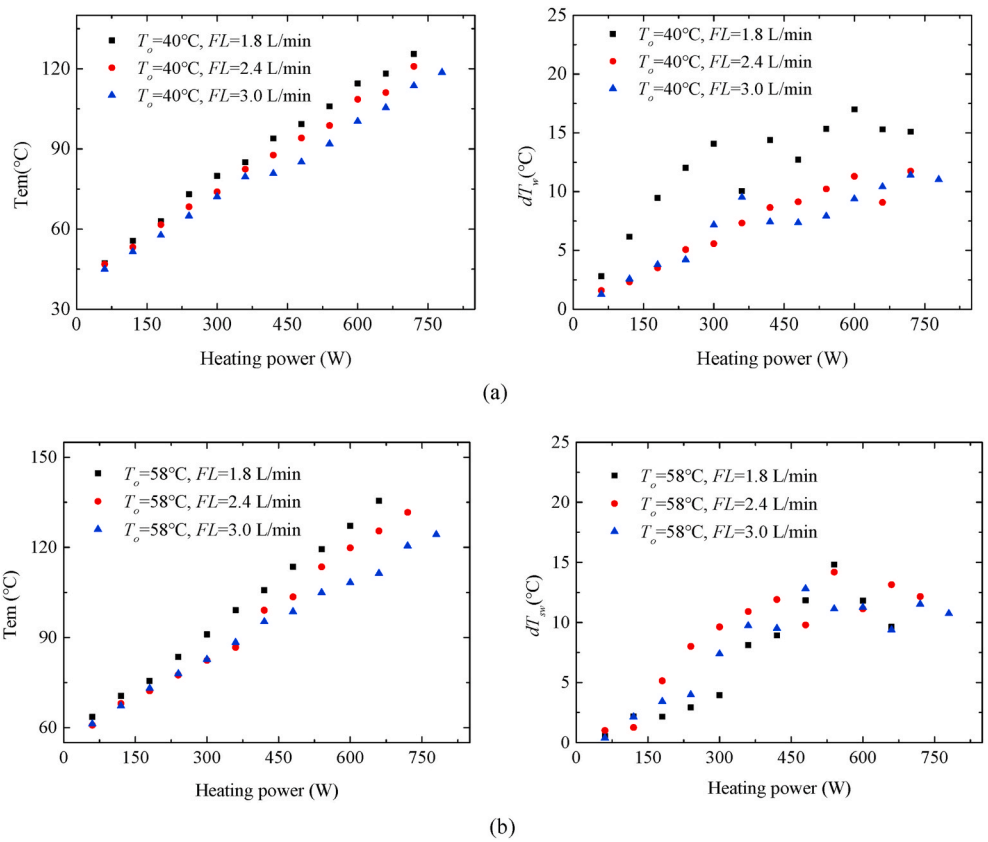

Fig. 2. The influence of oil flow rate on temperature and temperature gradient of slot winding with different oil temperatures (a) 40 °C; (b) 58 °C.

$$Nu = \frac{h_o d_n}{\lambda_o} \tag{4}$$

$$Re = \frac{V d_n}{\upsilon} \tag{5}$$

$$Pr = \frac{\upsilon}{a} \tag{6}$$

The heat transfer coefficient of the oil is correlated by,

$$h_o = \frac{Q_w}{A_{ew}(T_{ew} - T_{oil})} \tag{7}$$

The characteristic temperature to evaluate the thermodynamic properties of oil is the average temperature of end winding and oil. The velocity of the oil at the outlet of the nozzle is calculated by Ref. [31],

$$V = \sqrt{V_i^2 + \frac{2\Delta p}{\rho_l} - \frac{12\sigma}{\rho_l d_{32}}} \tag{8}$$

In the calculation, the influence of surface tension term and the inlet velocity are neglected, as their contribution is very minor. The uncertainties of the temperature difference and heat transfer coefficient are calculated by,

$$\delta y = \sqrt{\sum_{i=1}^{n} \left(\frac{\partial y}{\partial x_i}\right)^2 (\delta x_i)^2} \tag{9}$$

In this experiment, the maximum uncertainty of heat transfer coefficient was 6.25%.

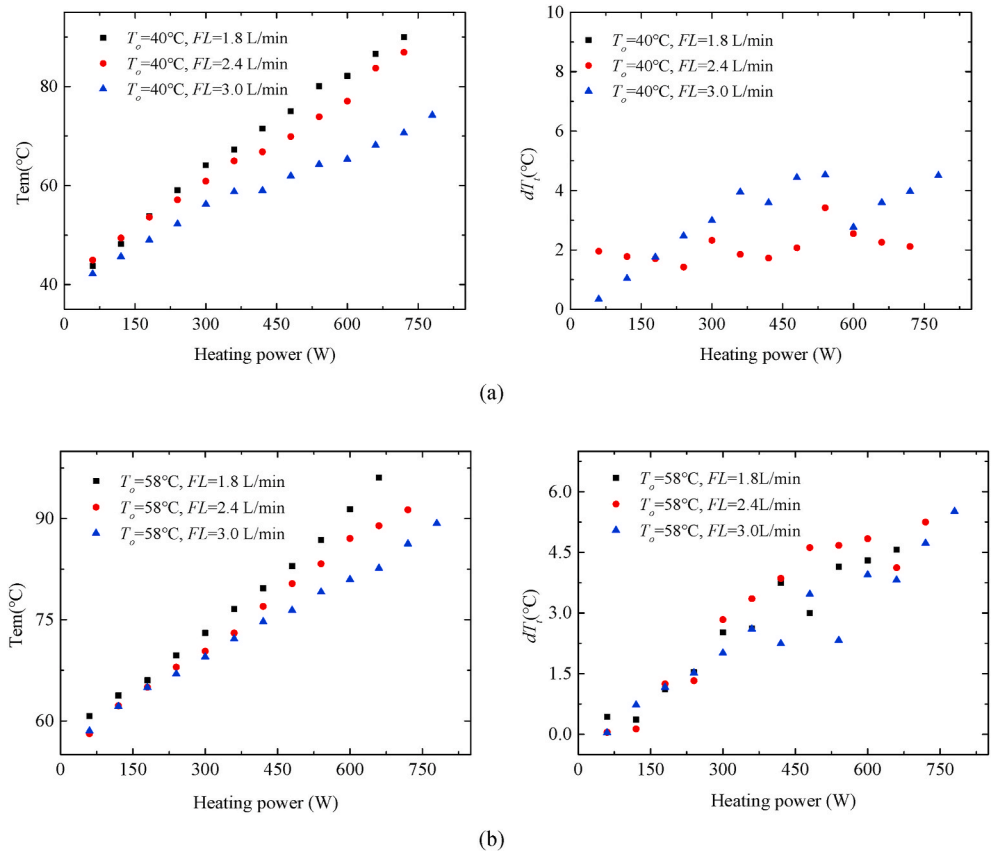

Fig. 3. The influence of oil flow rate on teeth and temperature gradient of teeth with different oil temperatures (a) 40 °C; (b) 58 °C.

3. Experimental results and discussions

3.1. The influence of oil flow rate

With the experimental rig above-mentioned, the influence of oil spray operational parameters was studied. Fig. 2 shows the temperature and temperature gradient of slot winding when the oil temperatures were 40 °C and 58 °C, respectively.

With the increase of the heating power, the temperature of the slot winding increased. With a higher oil flow rate, the temperature of the slot winding was lower than those of lower flow rates. When the heating power and oil temperature were 720 W and 40 °C, the temperature of the slot winding with 3.0 L/min was lower by 11.86 °C and 7.24 °C compared with those of 1.8 L/min and 2.4 L/min, respectively. It is because with a higher flow rate, more oil is pumped to the surface of end winding, thus the end winding is well covered and wetted by the oil. As a result, more heat is dissipated by the oil due to its larger heat capacity. Nevertheless, the advantage of a higher flow rate is not too obvious with relative lower heating power, as a low flow rate of oil is enough to dissipate the heat in this scenario. There is an apparent temperature gradient in the slot winding, as shown in Fig. 2. At oil temperature of 40 °C, with the increase of the oil flow rate, the temperature gradient of slot winding generally decreased. When the heating power and oil temperature were 600 W and 40 °C, the temperature gradient of the slot winding with 3.0 L/min was lower by 7.62 °C and 1.92 °C than those with 1.8 L/min and 2.4 L/min, respectively. However, the influence of oil flow rate on temperature gradient is not obvious with oil temperature of 58 °C. It also results from excellent heat-dissipation ability of higher oil flow rate.

The influence of oil flow rate on teeth temperature and teeth temperature gradient with oil temperature of 40 °C and 58 °C is presented in Fig. 3. Like slot winding, the temperature of the teeth also increased with the heating power. When the heating power was relatively lower, the influence of oil flow rate was not obvious. As for higher heating power, the temperature of the teeth was lower at a higher flow rate. While oil temperature and heating power were 58 °C and 660 W, the temperature of the teeth was 13.42 °C and 6.3 °C lower than those with 1.8 L/min and 2.4 L/min, respectively. The temperature gradient of the teeth is smaller than that of slot winding. The oil flow rate posed no obvious influence on the temperature gradient of the teeth.

3.2. The influence of oil temperature

The temperature of oil also has a great influence on the performance of spray cooling. The hydrodynamic and thermodynamic properties of oil, which directly affect the heat transfer, are highly dependent on temperature. Fig. 4 shows the influence of oil temperature on the temperature and temperature gradient of slot winding with different oil flow rates, oil temperatures and heating

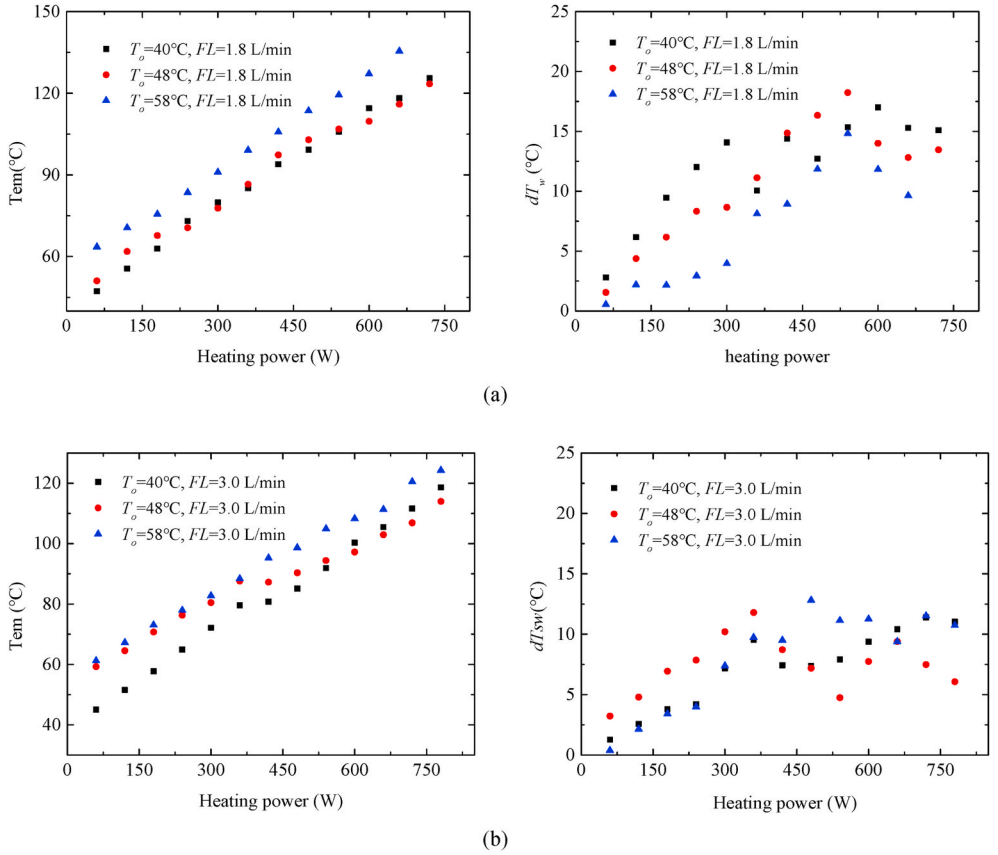

Fig. 4. The influence of oil temperature on temperature and temperature gradient of slot winding with different oil flow rates (a) 1.8 L/min; (b) 3.0 L/min.

powers. As can be seen, the temperature of slot winding increased with the heating power and oil temperature, while the temperature gradient increase first and then became flat. With the increase of oil temperature, the temperature gradient of slot winding decreased when the flow rate was 1.8 L/min at the heating power of 600 W, the temperature gradients were 17 K, 14 K and 11.8 K when the oil temperatures were 40 °C, 48 °C and 58 °C, respectively. Nevertheless, the temperature gradient was not sensitive to oil temperature when the flow rate was 3.0 L/min, which was caused by the excellent heat transfer ability of higher flow rate.

Fig. 5 presents the influence of oil temperature on teeth temperature and temperature gradient with different cooling conditions. The teeth temperature gradient firstly increased with heating power and the curve became flat. The temperature gradient of teeth was smaller than that of slot winding. The maximum temperature gradient within the testing range was 6.36 K when the oil temperature, oil flow rate and heating power were 48 °C, 1.8 L/min and 720 W, respectively. When the oil flow rate was 1.8 L/min, higher oil temperature generally achieved an even temperature distribution for the teeth. While the difference was not obvious with a flow rate of 3.0 L/min. For a smaller flow rate, the oil fluidity is very important, while the influence is not so greater with a higher oil flow rate. Thus, higher temperature of the oil is favorable because of lower viscosity.

3.3. Artificial neural network model for heat transfer coefficient

To precisely predict the heat transfer performance of oil spray, an artificial neural network (ANN) model was developed. In the ANN model, one hidden layer was used, and all neurons were connected, as shown in Fig. 6. The ANN model used Prandtl number and Reynolds number as inputs, and Nusselt number as output. All the data set were divided into three groups, and 70%, 15% and 15% of them were used as training, validation, and testing, respectively. In the proposed ANN model, the outputs of nodes are calculated by all its inputs along with their weights and biases, and given by,

$$\mathbf{y}^l = f\left(\sum_{j=1}^{n} \boldsymbol{\omega}^{l-1}\mathbf{x}^{l-1} + \mathbf{b}^l\right) \tag{10}$$

Therefore, the overall output of the proposed ANN model presented in Fig. 6 is given by Refs. [33,34],

$$\mathbf{y}_{pre} = f[\boldsymbol{\omega}^2(f(\mathbf{w}^1\mathbf{x}^1 + \mathbf{b}^1) + \mathbf{b}^2] \tag{11}$$

For all input data, the following function was used to pre-processes the input data,

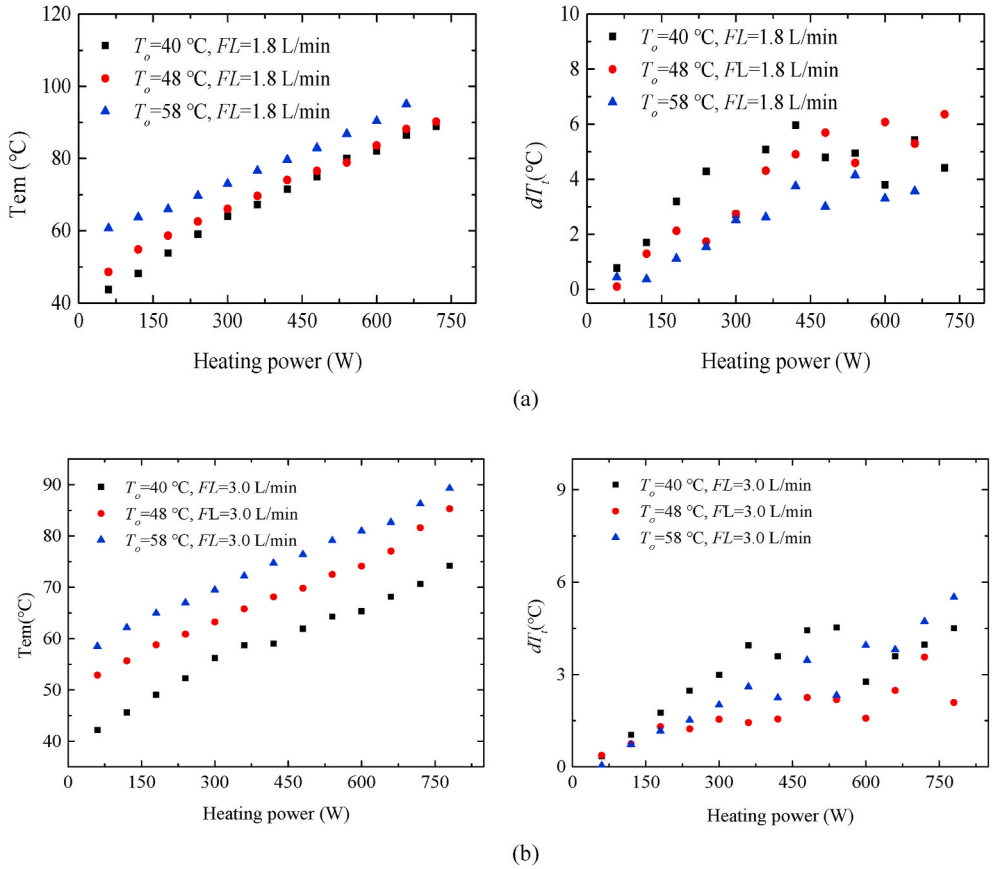

Fig. 5. The influence of oil temperature on temperature and temperature gradient of teeth with different oil flow rates (a) 1.8 L/min; (b) 3.0 L/min.

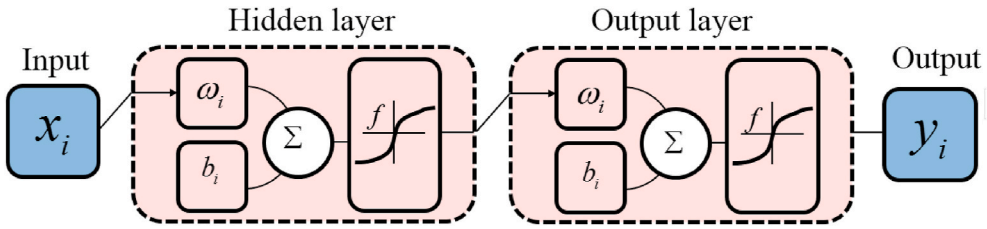

Fig. 6. The structure of ANN model.

$$\mathbf{y} = \frac{y_{\max} - y_{\min}}{x_{\max} - x_{\min}}(\mathbf{x} - x_{\min}) + y_{\min} \tag{12}$$

Due to its great adaptation and flexibility in non-linear ANN model, the Levenberg-Marquardt algorithm [32] was used to update the weights and biases of the ANN neurons. The Hessian matrix was approximated as,

$$H \approx J^T J \tag{13}$$

in which $\boldsymbol{J}$ is the Jacobian matrix, and presented by,

$$J = \begin{pmatrix} \frac{\partial e_1}{\partial p_1} & \frac{\partial e_1}{\partial p_2} & \cdots & \frac{\partial e_1}{\partial p_n} \\ \vdots & & \ddots & \vdots \\ \frac{\partial e_m}{\partial p_1} & \frac{\partial e_m}{\partial p_2} & \cdots & \frac{\partial e_m}{\partial p_n} \end{pmatrix} \tag{14}$$

To make sure the approximated Hessian matrix is invertible, it was further revised as,

$$H' = J^T J + \lambda E \tag{15}$$

Therefore, the update rule of Levenberg-Marquardt algorithm was given by Ref. [35],

$$p_{k+1} = p_k - H'^{-1} J_k e_k \tag{16}$$

For hidden layer, a sigmoid function was used as the activate function,

$$f_i(\mathbf{x}) = \frac{2}{1 + e^{-2\mathbf{x}_i}} - 1 \tag{17}$$

The cost function of the ANN model is defined by the following equation,

$$e = \frac{1}{2}\sum_{i=1}^{m}(y_i - y)^2 \tag{18}$$

To determine the neuron number of the hidden layer, a trial-and-error method was applied, and the result is shown in Fig. 7(a). When the neuron number was 8, the ANN model achieved a good balance between accuracy and complexity. Therefore, the structure of the ANN model proposed had 2 nodes, 8 nodes and 1 node in the input layer, hidden layer and output layer, respectively. The performance of ANN model is commonly evaluated by mean square error (MSE) and correlation coefficient. They are defined by,

$$MSE = \frac{1}{n_0}(\mathbf{y}_{pre} - \mathbf{y}_{exp})^{\mathrm{T}}(\mathbf{y}_{pre} - \mathbf{y}_{exp}) \tag{19}$$

$$r = \frac{\sum_{i=1}^{m}(x_i - \bar{x})(y_i - \bar{y})}{\sqrt{D(x)}\sqrt{D(y)}} \tag{20}$$

The performance of the ANN model is shown in Fig. 7 (b). The predicted Nusselt number coincided well with experimental data generally. The MSE and correlation coefficient of the model were 7.28 and 0.93, respectively. The optimized weights and biases are presented in Table 3.

4. Conclusion

In this paper, an innovative experimental study on the cooling performance of oil spray for end winding was conducted to address the challenge of higher heat flux of electric motors. Based on the experimental rig built, the influence of oil flow rate and oil temperature were studied. It was shown that with higher oil temperature and larger oil flow rate, lower temperatures of winding and teeth were achieved, as well as smaller temperature gradients in them. To correlate the experimental data, a fully-connected feedforward ANN model was further developed to predict the heat transfer performance of oil spray on end winding. There were 2 nodes, 8 nodes

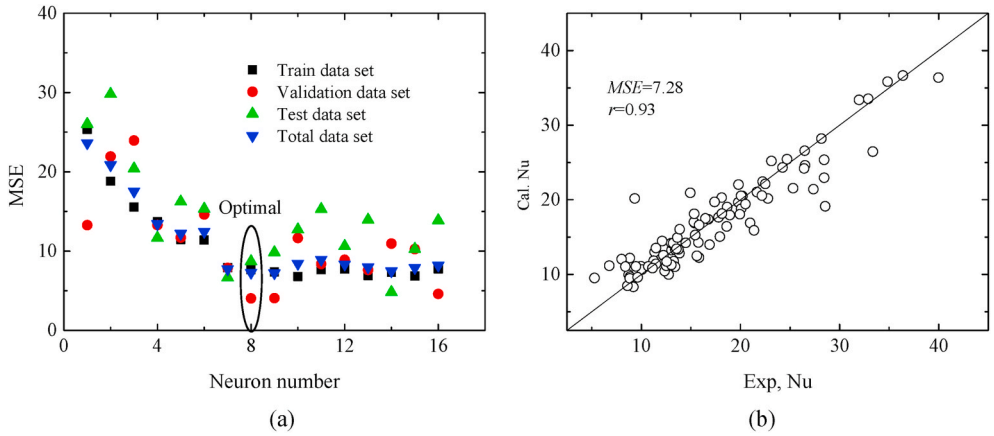

Fig. 7. ANN model for heat transfer performance (a) hidden layer neuron number optimization; (b) prediction performance of ANN model.

Table 3
Optimal weights and biases of ANN model.

Node	Hidden layer		Hidden layer bias	Output layer weight	Output layer bias
	Re	Pr			
1	1.9867	2.2583	−1.3510	−1.3543	−0.6689
2	−4.0809	0.2674	2.5835	6.3306	
3	5.0819	1.2304	−2.0409	6.4656	
4	0.2467	1.6672	−1.4096	1.8991	
5	0.8209	22.661	11.7817	−3.4115	
6	0.0586	−17.700	−9.1988	−3.1278	
7	5.8845	−1.8555	6.6334	0.5460	
8	1.7607	13.917	−9.7906	−0.2917	

and 1 node in input layer, hidden layer and output layer, respectively. The predicted results of the model coincided with experimental data very well with the MSE and correlation coefficient of 7.28 and 0.93, respectively. The optimized biases and weights were given for future designs and applications.

Despite the current research is expected to be a good reference for the future research, more studies regarding wider operating conditions, various end winding configurations, different types of motors as well as fundamental revealing on spray heat transfer characteristics, will surely benefit both the industrial applications and scientific exploration.

Declare of interest

None.

Author statement

Xuehui Wang: Conceptualisation, Experimental testing, ANN modelling and analysis, Writing – original draft, response to comments. **Bo Li:** Experimental preparation, attending experimental testing, testing data reviewing. **Kuo Huang:** Experimental preparation, Attending testing, and testing data reviewing. **Yuying Yan:** Conceptualisation, Funding acquisition, Analysis, Supervision, Writing – review & editing, response to comments. **Ian Stone**: conceptualisation discussion, testing data analysis & reviewing, Writing – review. **Sean Worrall**: Conceptualisation discussion, testing data analysis & reviewing.

Declaration of competing interest

The authors declare that they have no known competing financial interests or personal relationships that could have appeared to influence the work reported in this paper.

Acknowledgement

This work was financially sponsored by the following research grants: H2020-MSCA-RISE-778104 – ThermaSMART, and Innovate UK (AceDrive No. 113167).

References

[1] D. Tran, M. Vafaeipour, M. El Baghdadi, et al., Thorough state-of-the-art analysis of electric and hybrid vehicle powertrains: topologies and integrated energy management strategies [J], Renew. Sustain. Energy Rev. 119 (2020), 109596.
[2] M. Salvia, D. Reckien, F. Pietrapertosa, et al., Will climate mitigation ambitions lead to carbon neutrality? An analysis of the local-level plans of 327 cities in the EU [J], Renew. Sustain. Energy Rev. 135 (2021), 110253.
[3] F. Schreyer, G. Luderer, R. Rodrigues, et al., Common but differentiated leadership: strategies and challenges for carbon neutrality by 2050 across industrialized economies [J], Environ. Res. Lett. 15 (11) (2020).
[4] J. Liang, Y. Gan, Y. Li, Investigation on the thermal performance of a battery thermal management system using heat pipe under different ambient temperatures [J], Energy Convers. Manag. 155 (2018) 1–9.
[5] Y. Gan, J. Wang, J. Liang, et al., Development of thermal equivalent circuit model of heat pipe-based thermal management system for a battery module with cylindrical cells [J], Appl. Therm. Eng. 164 (2020), 114523.
[6] Global_EV_Outlook_2021, Technology Report, published by International Energy Agency (IEA), April 2021, https://www.iea.org/reports/global-ev-outlook-2021.
[7] G. Du, W. Xu, J. Zhu, et al., Power loss and thermal analysis for high-power high-speed permanent magnet machines [J], IEEE Trans. Ind. Electron. 67 (4) (2020) 2722–2733.
[8] X. Wang, B. Li, D. Gerada, K. Huang, I. Stone, S. Worrall, Y. Yan, A critical review on thermal management technologies for motors in electric cars [J], Appl. Therm. Eng. 201 (2021), 117758.
[9] J. Wang, Y. Gan, J. Liang, et al., Sensitivity analysis of factors influencing a heat pipe-based thermal management system for a battery module with cylindrical cells [J], Appl. Therm. Eng. 151 (2019) 475–485.
[10] B. Li, Kuo Huang, X. Wang, et al., Thermal management of electrified propulsion system for low-carbon vehicles [J], Autom. Innovat 3 (4) (2020) 299–316.
[11] C. Kim, K. Lee, S. Yook, Effect of air-gap fans on cooling of windings in a large-capacity, high-speed induction motor [J], Appl. Therm. Eng. 100 (2016) 658–667.
[12] Putra Nandy, Bambang Ariantara, Electric motor thermal management system using L-shaped flat heat pipes [J], Appl. Therm. Eng. 126 (2017) 1156–1163.
[13] A. Tuysuz, F. Meyer, M. Steichen, et al., Advanced cooling methods for high-speed electrical machines [J], IEEE Trans. Ind. Appl. 53 (3) (2017) 2077–2087.
[14] M. Grabowski, K. Urbaniec, J. Wernik, et al., Numerical simulation and experimental verification of heat transfer from a finned housing of an electric motor [J], Energy Convers. Manag. 125 (2016) 91–96.
[15] S. Ulbrich, J. Kopte, J. Proske, Cooling fin optimization on a TEFC electrical machine housing using a 2-D conjugate heat transfer model [J], IEEE Trans. Ind. Electron. 65 (2) (2018) 1711–1718.
[16] H. Peng, F. Lai, Investigation of parameters affecting heat transfer and fluid flow of a TEFC electric motor by using taguchi method [J], IOP Conf. Ser. Mater. Sci. Eng. 491 (2019) 12021.
[17] A. Fasquelle, D. Laloy, Water cold plates cooling in a permanent magnet synchronous motor [J], IEEE Trans. Ind. Appl. 53 (5) (2017) 4406–4413.
[18] J. Li, Y. Lu, Y. Cho, et al., Design, analysis, and prototyping of a water-cooled axial-flux permanent-magnet machine for large-power direct-driven applications [J], IEEE Trans. Ind. Appl. 55 (4) (2019) 3555–3565.
[19] P. Wu, M. Hsieh, W.L. Cai, et al., Heat transfer and thermal management of interior permanent magnet synchronous electric motor [J], Inventions 4 (4) (2019) 69.
[20] M. Satrústegui, M. Martinez-Iturralde, J.C. Ramos, et al., Design criteria for water cooled systems of induction machines[J], Appl. Therm. Eng. 114 (2017) 1018–1028.
[21] P. Lindh, I. Petrov, J. Pyrhonen, et al., Direct liquid cooling method verified with a permanent-magnet traction motor in a bus [J], IEEE Trans. Ind. Appl. 55 (4) (2019) 4183–4191.
[22] Z. Liu, T. Winter, M. Schier, in: Comparison of Thermal Performance between Direct Coil Cooling and Water Jacket Cooling for Electric Traction Motor Based on Lumped Parameter Thermal Network and Experimentation: EVS28 International Electric Vehicle Symposium and Exhibition, Kintex Korea, 2015 [C].
[23] A. Reinap, F.J. Marquez-Fernandez, M. Alakula, et al., in: Direct Conductor Cooling in Concentrated Windings: XIII International Conference on Electrical Machines (ICEM), Alexandroupoli, Greece, 2018 [C].
[24] Z. Xu, A. Timimy, M. Degano, et al., in: Thermal Management of a Permanent Magnet Motor for an Directly Coupled Pump: XXII International Conference on Electrical Machines, ICEM), Lausanne, Switzerland, 2016 [C].
[25] Y. Li, T. Fan, W. Sun, et al., in: Experimental Research on the Oil Cooling of the End Winding of the Motor: IEEE Energy Conversion Congress and Exposition, ECCE), Milwaukee, WI, USA, 2016 [C].
[26] V. Madonna, A. Walker, P. Giangrande, et al., Improved thermal management and analysis for stator end-windings of electrical machines [J], IEEE Trans. Ind. Electron. 66 (7) (2019) 5057–5069.
[27] V. Madonna, P. Giangrande, A. Walker, et al., in: On the Effects of Advanced End-Winding Cooling on the Design and Performance of Electrical Machines: XIII International Conference on Electrical Machines (ICEM), Alexandroupoli, Greece, 2018 [C].
[28] C. Liu, H. Zhang, Z. Xu, et al., Experimental investigation on oil spray cooling with hairpin windings [J], IEEE Trans. Ind. Electron. (2019) 1–11.
[29] Y. Li, T. Fan, Q. Li, et al., Experimental Investigation on Heat Transfer of Directly-Oil-Cooled Permanent Magnet Motor: 19th International Conference on Electrical Machines and Systems (ICEMS), Chiba, Japan, 2016 [C].
[30] M.R. Guechi, P. Desevaux, P. Baucour, et al., Spray cooling of electric motor coil windings [J], J. Comput. Multiph. Flows 8 (2) (2016) 95–100.
[31] W. Zhang, Z. Wang, Heat transfer enhancement of spray cooling in straight-grooved surfaces in the non-boiling regime, Exp. Therm. Fluid Sci. 69 (2015) 38–44.
[32] J. Bilski, B. Kowalczyk, A. Marchlewska, et al., Local levenberg-marquardt algorithm for learning feedforwad neural networks [J], J. Artif. Intell. Soft Comput. Res. 10 (4) (2020) 299–316.
[33] X. Wang, Y. Yan, X. Meng, et al., A general method to predict the performance of closed pulsating heat pipe by artificial neural network [J], Appl. Therm. Eng. 157 (2019), 113761.
[34] X. Wang, X. Yan, N. Gao, et al., Prediction of thermal conductivity of various nanofluids with ethylene glycol using artificial neural network [J], J. Therm. Sci. 29 (2020) 1504–1512.
[35] X. Wang, E. Wright, Z. Liu, et al., Development of a novel artificial neural network model for closed pulsating heat pipe with water and aqueous solutions, [J] 17 (1) (2021), e2719.